Dynamics of a Dual Offshore Renewable Energy System: Analysis of Wind and Tidal Turbine

Talal Mohamed Al Hajeri BEng Naval Architecture and Marine Engineering with Honours; MSc Chemical Engineering; MSc Petroleum Engineering
Khalifa University of Science and Technology and Research
(of Affiliation)
Abu Dhabi, United Arab Emirates
talal.alhajeri@ku.ac.ae

1 Synopsis

Offshore renewable energy has been showing remarkable growth and acceptable yields over recent years, the concept of this study centers on the idea of connecting a wind turbine to a tidal turbine, where both energy sources may be utilized at any one location for maximum energy yield. AutoCAD and MATHCAD have been used to simulate the aerodynamics and hydrodynamics of the structure. The power generation and risk analysis were also accounted for. The result of a wave spectral analysis effect on tidal turbines is demonstrated in the study for 6 different cases at different mean crossing period, wave heights, and fatigue life. The power generation of 2 bladed wind/tidal turbine versus 3 bladed was calculated. Although 3 bladed turbines have a marginal higher power generation output, this does not reflect the feasibility of the extra percentages of power on the economics.

Keywords— Bernoulli's Equation, Morrison's Equation, Drag Coefficient, Lift Coefficient, Navier-Stokes

2 Introduction

2.1 Number of Blades

A two bladed wind turbines (2BWT) rotor is located downwind. The connection of the rotor to the shaft is through a hinge (teeter mechanism) which omits the presence of any bending moments which may be transmitted from the rotor to the shaft making it more flexible than the three bladed wind turbines (3BWT) (Wilson and Lissaman 1974; Ahlstrom 2005; Hansen 2008; Hayat et al. 2019). Since bending moments are never present on this system it is likely that there won't be any requirement in installing devices that will reduce the bending moments, the device could be built lighter and smaller thus adding to the advantages of being cheaper.

Rotors with less than three blades have the tendency to generate considerable alternating loads with respect to the yaw moments and the drive torque. however, the rotor moments balance out in every revolution for rotors with more than two blades. The dynamic response of the rotor is another factor which is associated with the number of blades, there will be deformations experienced by the rotating rotor which are influenced by external forces acting on the rotor such as bending of the blades. This in turn will produce inertial forces because of the accelerating masses of the blades. (Gamett 1960; Wilson and Lissaman 1974; NASA 1979; Sundar and Sullivan 1982; Ahlstrom 2005; Hau 2006; Hansen 2008; Hayat et al. 2019)

2.2 Aerodynamics

The amount of power depends on the aerodynamic forces utilized for producing this power as well as geographical location, number of blades, height above ground level, etc. The maximum mechanical wind energy which can be extracted from any cross section is limited to 0.593 (*Betz's limit*) or 60% of the total wind energy can be utilized for useful purposes (Wilson and Lissaman 1974; Gilbert and Foreman 1983; Hansen et al. 2000; Hau 2006; Bianchi et al. 2007; Hansen 2008).

According to the *Blade Element Theory* surfaces exposed to an airflow stream are inadvertently subjected to aerodynamic forces the components of which are, *Drag* (D) which acts in the direction of the flow, and *Lift* (L) which acts in the direction perpendicular to the flow. (Wilson and Lissaman 1974; NASA 1979; Sundar and Sullivan 1982; Gilbert and Foreman 1983; Hansen et al. 2000a,

 http://doi.org/10.24868/icmet.oman.2019.024

2005b; Ahlstrom 2005; Hau 2006; Bianchi et al. 2007; Hansen 2008; Lin and Sayer 2015; Hayat et al. 2019).

$$C_l = \frac{L}{\frac{1}{2}\rho {V_\infty}^2 c} \quad \textbf{(1)}$$

$$C_d = \frac{D}{\frac{1}{2}\rho {V_\infty}^2 c} \quad \textbf{(2)}$$

Where C_l is the lift coefficient, C_d is the drag coefficient, V_∞^2 is the velocity relative to the angle of the blade, c is the chord length. pure drag, involves airflow at a specific velocity pushing a surface of known area around a revolving tower (Lissaman 1979; Hau 2006). Lift forces in contact with the blades are subdivided into the tangential component in the plane of rotation of the rotor known as *Torque*, and a component perpendicular to the plane of rotation known as *thrust*. The lift concept yields higher power coefficients which can reach values of up to 0.5.

The design of wind turbine blades is based on the load spectrum applied with respect to fatigue strength, and the mathematical modeling for the dimensioning of the structure which is stressed dynamically (Gamett 1960; NASA 1979; Ainsile 1988; Hau 2006; Hayat et al. 2019).

3 Aerodynamics of Wind

3.1 Yaw Control Mechanism

The wind changes direction all the time there will be times when the wind direction is not normal to the rotor plane but at an angle, and at these angles the amount of wind captured is reduced. To counter this a *yaw mechanism* is used to position the turbine normal to the wind. the angle required to steer the rotor plane into the wind is known as the *Yaw Angle* which is done using the following techniques. (NASA 1979; Hayat et al. 2019).

1. Aerodynamic yaw using wind vanes or fan tail wheels
2. Free yawing
3. Active yawing using a motorized yaw drive

3.2 Forces on a Cylinder

The wind speed will decrease significantly as it rubs around the outer layer of the structure. Another reason for speed reduction is because of the internal friction contained in the flowing medium, as well as the surface friction of the encountered body causes the flow to separate past the structure over what is known as the *wake-area*. The wake-area is characterized by turbulence and a reduced mean flow velocity there will be alternating vortices (*Karman Vortices*) on both sides of the cylinder occurring at a defined frequency (Hau 2006; Hayat et al. 2019).

The mathematical modeling of the wake has been first attempted by *Lissaman* in 1977 with the development of the wake profile (Lissaman 1979; Hau 2006).

The area close to the rotor is determined by pressure equalization with the ambient air directly after the rotor and by vortex wakes generated by flow around rotor blades. There will be pressure differences which will cause wake area to widen. Further away from the wake's center the velocity profile develops into a *Gaussian Distribution* **(**Hau 2006; Wang and Low 2019).

In the case of waves and current the fluid forces which contribute to the mean resultant force are the *Friction Force* and the *Pressure Force* (Sarpkaya 1979; Sumer and Fredsoe 2006; Giorgi and Ringwood 2017a, 2018b).

$$\bar{F}_p = \int_0^{2\pi} \bar{p}\cos(\phi) r_0 d\phi \quad \textbf{(3)}$$

$$\bar{F}_f = \int_0^{2\pi} \bar{\tau}_0 \sin(\phi) r_0 d\phi \quad \textbf{(4)}$$

$$\bar{F}_D = \bar{F}_p + \bar{F}_f \quad \textbf{(5)}$$

Where $\bar{p}$ is the pressure and $\bar{\tau}_0$ is the wall shear stress on the cylinder surface, and the overbar denotes time averaging. $\bar{F}_p$ Is termed the *Form Drag*, $\bar{F}_f$ is the *Friction Drag*, and $\bar{F}_D$ is the *Mean Drag*.

$$\bar{F}_D \cong \int_0^{2\pi} \bar{p}\cos(\phi) r_0 d\phi \quad \textbf{(6)}$$

With increasing or decreasing values of Re, $\bar{C}_D$ exhibits a similar behavior. At the supercritical the $\bar{C}_D$ is approximately 1.2, and when Re drops to the so called subcritical the $\bar{C}_D$ drops drastically to 0.25 For a rough cylinder $\bar{C}_D$ becomes a factor of not just Re but also of the roughness parameter (k_s/D); where k_s is the Nikuradse equivalent sand roughness (Achenback 1968; Guven et al. 1980; Hau 2006; Sumer and Fredsoe 2006).

$$\bar{C}_D = \bar{C}_D\left(Re, \frac{k_s}{D}\right) \quad \textbf{(7)}$$

4 Hydrodynamics of Waves and Current

Sinusoidal waves are symmetric and do not represent themselves with the sharp crest, shallow trough shapes as trochoidal waves do**.** Moreover, sinusoidal waves generate pressure, velocity, and vortices distributions which concur with actual values generated from studies**.** By adding various sinusoidal waves of different frequencies, heights, and travelling in different directions an actual sea state can be created (Newman 1977; Ruzzo et al. 2019).

$$\xi = a\sin(kx - \omega t) \quad \textbf{(8)}$$

The wave profile can be written as seen in equation 8, where ξ is the wave elevation, a is the wave amplitude, ω is the wave frequency, k is the wave number, x is the direction of propagation and t is for time. Fluids are characterized as *Incompressible* imply that however the amount of fluid flowing into the region it must be matched by an equal amount flowing out (Jordan and Fromm 1972; Sarpkaya 1989; Deng et al. 2019; Lee et al. 2019; Li and Liu 2019; Wang et al. 2019).

For a 2D rectangular region the inlet and outlet flow are components u and v in the horizontal and vertical direction which are perpendicular to each other. Since the area of the rectangle is non-zero, the *Continuity Equation* can be written as follow: (Christiansen 1971; Newman 1977; Zhang and Dalton 1992; Sumer and Fredsoe 2006; Perić and Abdel-Maksoud 2015; Aggarwal et al. 2016; Stepanov and Trevisan 2016).

$$\frac{\partial u}{\partial x} + \frac{\partial v}{\partial y} = 0 \quad \textbf{(9)}$$

From equation 9 of the continuity equation the first term *du/dx* represents the x-velocity component and *dv/dy* is the y-velocity component of the flow. The actual motion of a fluid particle has a translational motion and a rotational motion. The first has to do with the distance travelled by the center of gravity, and the latter represents the spin of the fluid particle about its center of gravity (Zhang and Dalton 1992). If all external forces are neglected this gives rise to *Viscosity* which can generate shear forces, and cause the fluid particle to spin (Aggarwal et al. 2016; Lee et al. 2019). For an inviscid flow there is no spin observed by the fluid particle, this helps in defining the velocity potential which represents the stream as an *Irrotational Flow* (Newman 1977; Li and Liu 2019).

$$w = \frac{\partial v}{\partial x} - \frac{\partial u}{\partial y} \quad \textbf{(10)}$$

Equation 10 takes the difference between the vertical and horizontal components of the flow and gives rise to the *vorticity* term *w*. From the velocity potential the pressure, wave directional velocities, wave directional acceleration may be calculated leading to forces and moments. The velocity potential is defined as $Velocity \times Distance$ which is path independent (Newman 1977; Sarpkaya 1979a, 1989b; Leonard 1980; Sumer and Fredsoe 2006; Li and Liu 2019).

$$\emptyset = -\frac{ga}{\omega} e^{kz} \cos(kx - \omega t) \quad \textbf{(11)}$$

Equation 11 shows the velocity potential in deep water where all the terms are similar to equation 8 with the addition of the gravity term *g* and *z* which is related to depth. In general fluid motion there will be alternations in the velocity potential and pressure which do depend on the path taken. The *Circulation* which is the integral of the velocity potential around any closed path becomes relevant. Vorticity of the flow is obtained by dividing the circulation by the area enclosed (Sarpkaya 1989). Therefore, if the flow is irrotational then naturally the vorticity is zero, and vice versa (Christiansen 1971; Newman 1977; Leonard 1980; Sumer and Fredsoe 2006).

4.1 Bernoulli's Equation

Bernoulli's equation with the absence of any external forces such as gravity represented as follow: (Newman 1977; Sumer and Fredsoe 2006; Vasan and Deconinck 2012; Li and Liu 2019).

$$P + \frac{1}{2}\rho u^2 = constant \quad \textbf{(12)}$$

Where *P* is the static pressure of the fluid at the cross section, ρ is the fluid density, and *u* is the mean velocity of the fluid flow. The free water surface is where the effects of wave are greatest and at this point the velocity potential always occurs. At the free surface the pressure must remain constant and equal to the atmospheric pressure, this can be expressed in the extended form of the Bernoulli's equation where hydrostatic and hydrodynamic pressures are involved as well as the presence of the wave (Newman,1977;

Sarpkaya 1979; Barltrop and Adams 1991; Vasan and Deconinck 2012; Wang and Low 2019).

$$P = constant - \frac{1}{2}\rho(u^2 + w^2) - \rho g z - \rho\frac{\partial \emptyset}{\partial t} \qquad \textbf{(13)}$$

Equation 13 shows the extended form of the Bernoulli's equation where the second term denote the nonlinear quadratic pressure, followed by the hydrostatic pressure, and the hydrodynamic pressure.

4.2 Morrison's Equation

From Bernoulli's equation, the overall pressure comprises of the hydrostatic and the hydrodynamic pressures. As a wave comes in contact with a body there will be disturbances in the local pressure field which would cause some of the energy contained within it to be reflected, deflected, and or scattered, this is generally known as *Diffraction* (Maull and Milliner 1978; Barltrop and Adams 1991; Li and Liu 2019; Wang et al. 2019; Wu and Lin 2019). If the geometry of the body is considerably smaller than the wavelength then diffraction may be neglected, and only the velocity potential of the undisturbed incident wave is considered for results (Resio et al. 2015).

In the case of the wind/tidal turbine tower, the diameter of the structure is assumed to be smaller than the wavelength. This brings forth the *Morrison's Equation* which has been developed by J R Morison, to strictly model the hydrodynamic forces exerted on offshore vertical towers.

$$F(t) = C_M \underbrace{\overbrace{\rho\forall}^{mass}}_{Froude}\ \underbrace{\overbrace{\dot{v}(t)}^{acceleration}}_{Krylov} + C_D\frac{1}{2}\rho A v(t)|v(t)| \qquad \textbf{(14)}$$

Where C_M and C_D are the Morrison's inertia and drag coefficient, V is the displaced volume, ρ is the density, and A is the projected area in the wave direction (Newman 1977; Maull and Milliner 1978; Sarpkaya 1979; Barltrop and Adams 1991; Sumer and Fredsoe 2006; Aggarwal et al. 2016).

The equation works well when $D/\lambda \leq 0.2$, i.e when diffraction is minimal and the equation tends to lose its credibility when that value is exceeded (Newman 1977; Barltrop and Adams 1991).

The hydrodynamic Mass (m') or (ρV) from Morrison's equation is the mass of the fluid around the body which is accelerated with the movement of the body due to the action of pressure (Newman 1977; Sumer and Fredsoe 2006). The m' is estimated by neglecting all frictional effects, in other words the flow is calculated by equilibrium of the fluid force between pressure and inertia (*Potential Flow Theory*).

The drag depends on factors such as the geometry and the hydrodynamics. The drag force is related to the wave loading on the structure and is more dominant in extreme waves (Newman 1977; Maull and Milliner 1978; Sarpkaya 1979; Barltrop and Adams 1991; Sumer and Fredsoe 2006; Cao et al. 2014; Aggarwal et al. 2016; Giorgi and Ringwood 2018; Wu and Lin 2019).

The inertia is made up of the *Froude-Krylov Force* and the fact that the structure feels the effects of the wave acceleration even if the waves did not feel the presence of the structure The inertia force becomes vital when looking at smaller waves, and is especially important in fatigue analysis (Sarpkaya 1979; Barltrop and Adams 1991; Sumer and Fredsoe 2006; Cao et al. 2014; Rodrigues and Soares 2017; Giorgi and Ringwood 2018; Beji 2019; Deng et al. 2019; Li and Liu 2019; Ruzzo et al. 2019; Wu and Lin 2019).

Measuring C_D and C_M depends on the Reynolds number (Re) and the Keulegan-Carpenter number (KC) which are normally obtained through experimentation. Another technique used to determine the force coefficients is the *Method of Least Squares* where C_D and C_M are determined by the mean-squared difference between the predicted by Morrison's equation and measured force. (Sumer and Fredsoe 2006; An et al. 2010; Cao et al. 2014; Lin and Sheng 2017).

$$C_D = \frac{8}{3\pi}\frac{1}{\rho D U_m^2}\int_0^{2\pi} F_m \cos(\omega t)\,|\cos(\omega t)|\,d(\omega t) \qquad \textbf{(15)}$$

$$C_M = \frac{2KC}{\pi^3}\frac{1}{\rho D U_m^2}\int_0^{2\pi} F_m \sin(\omega t)\,d(\omega t) \qquad \textbf{(16)}$$

Where U_m is the wave velocity and F_m is the measure in-line force. Another method which depends on experimentation results of C_D and C_M is by using the *Fourier series*. This technique gives C_M similar to those given by the least square method, as for C_D the values are slightly different than those given by the least square method. (Maull and Milliner 1978; Sumer and Fredsoe 2006; Aggarwal et al. 2016; Lin et al. 2017; Rodrigues and Soares 2017; Lee et al. 2019).

Experiments show that friction is significant at small KC numbers; in fact, the portion of total drag influenced by friction is approximately 50% for $KC = 0$ or 1(Zhang and Dalton 1992). At KC = 6

the friction drag portion of the total drag decreases to about 10%. For C_M the friction generated inertia force is a small fraction of the total inertia force and may therefore be neglected in most cases (Maull and Milliner 1978; Zhang and Dalton 1992; Sumer and Fredsoe 2006; Cao et al. 2014).

4.3 Navier-Strokes Equation

For extreme sea states or when greater order accuracy is needed, it becomes favorable to use a higher order non-linear equation such as *Navier-Strokes Equation*

$$\frac{D\underline{V}}{Dt} = -\frac{1}{\rho}\nabla P + \nu\nabla^2\underline{V} \quad \textbf{(17)}$$

Where $\underline{V}$ is the velocity vector, P is the pressure, ρ is the density, and ν is the kinematic viscosity of the fluid, D/Dt is the total derivative i.e. $\frac{D}{Dt} = \frac{\partial}{\partial t} + \underline{V}\nabla$ (Hansen et al. 1997; Leonard 1980; Chaviaropoulos and Hansen 2000; Hansen et al. 2006; Sumer and Fredsoe 2006; An et al. 2010; Cao et al. 2014; Perić and Abdel-Maksoud 2015; Kaffash et al. 2017; Deng et al. 2019; Lee et al. 2019).

4.4 Froude Krylov and Added Mass

To work out the *Froude-Krylov* forces the distribution of the hydrodynamic pressure around a circular cylinder must be obtained and then integrate to find the force. In various books, and journals this technique is referred to as the *Pressure x Area* method (Giorgi and Ringwood 2017a, 2018b; Beji 2019).

Another method which is more frequently used as a form of the Morrison's equation and which is associated with Newton's second law is the $Mass \times Acceleration$. Here the acceleration is assumed constant around the circular cylinder, and mass is the only variable that determines the magnitude of the force, unlike the $Pressure \times Area$ where the shape of the cylinder plays a role (Sarpkaya 1979). The shape of the circular cylinder is considered and verified by the *Added mass* (C_A) and C_D.

$$F = \frac{1}{2}\rho C_D(U - U_b)|U - U_b| + \rho C_A A\left(\dot{U} - \dot{U}_b\right) + \rho A\dot{U} \quad \textbf{(18)}$$

C_A depends on wave parameters, and the geometry of the submerged part of the structure. C_A is paramount for calculating the inertia force in the Morrison's equation and in practical application is multiplied by the Froude-Krylov force once it has been integrated. It follows from the equation that $C_M = 1 + C_A$ where both coefficients are frequency dependent and can be obtained from tables of coefficient on structures of various cross-sections and thicknesses (Newman 1977; Barltrop and Adams 1991; Sumer and Fredsoe 2006; Giorgi and Ringwood 2017a, 2018b).

5 AutoCAD Modelling

5.1 Wind Turbine Particulars

Number of Units	= 1
Number of Blades	= 3
Rotor Diameter	= 40 (m)
Hub Diameter	= 4 (m)
Blade Length	= 18 (m)
Blade Chord Length (Root)	= 2 (m)
Blade Chord Length (Tip)	= 0.5 (m)
Blade Max Thickness	= 0.75 (m)
Blade Pitch Angle	= -2°
Blade Twist Angle	= variable
Nacelle	= at tower top

5.2 Tidal Turbine Particulars

Number of Units	= 2
Number of Blades	= 3
Rotor Diameter	= 12 (m)
Hub Diameter	= 2 (m)
Hub Depth	= 8…12 (m) below sea level
Blade Length	= 5 (m)
Blade Chord Length (Root)	= 1 (m)
Blade Chord Length (Tip)	= 0.25 (m)
Blade Max Thickness	= 0.50 (m)
Blade Pitch Angle	= -2°
Blade Twist Angle	= variable
Nacelle	= 20 m above sea level

5.3 Tower Particulars

Tower Height	= 80 (m)
Tower Air Draught	= 60 (m)
Tower Deep Draught	= 20 (m)
Tower Diameter	= 4 (m)
Foundation Diameter	= 20 (m)
Foundation Thickness	= 2 (m)

5.4 Environmental Particulars

Wind Velocity	= 1…25 (m/s)
Wind Density	= 1.25 (kg/m^3)

Wind Kinematic Viscosity	= 1.5 * 10^{-5} (m^2/s)
Min Air Reynolds Number	= 1.33 * 10^5
Max Air Reynold's Number	= 3.33 * 10^6
Wave Height	= 3.5 (m)
Wave Velocity	= 1…25 (m/s)
Water Density	= 1025 (kg/m^3)
Water Kinematic Viscosity	= 9.02 * 10^{-5} (m^2/s)
Min Water Reynolds Number	= 1.11 * 10^4
Max Water Reynold's Number	= 2.77 * 10^5
Tidal Height	= NA
Tidal Velocity	= NA
Water Depth	= 20 (m)
Distance From Shore	= 10 (km)

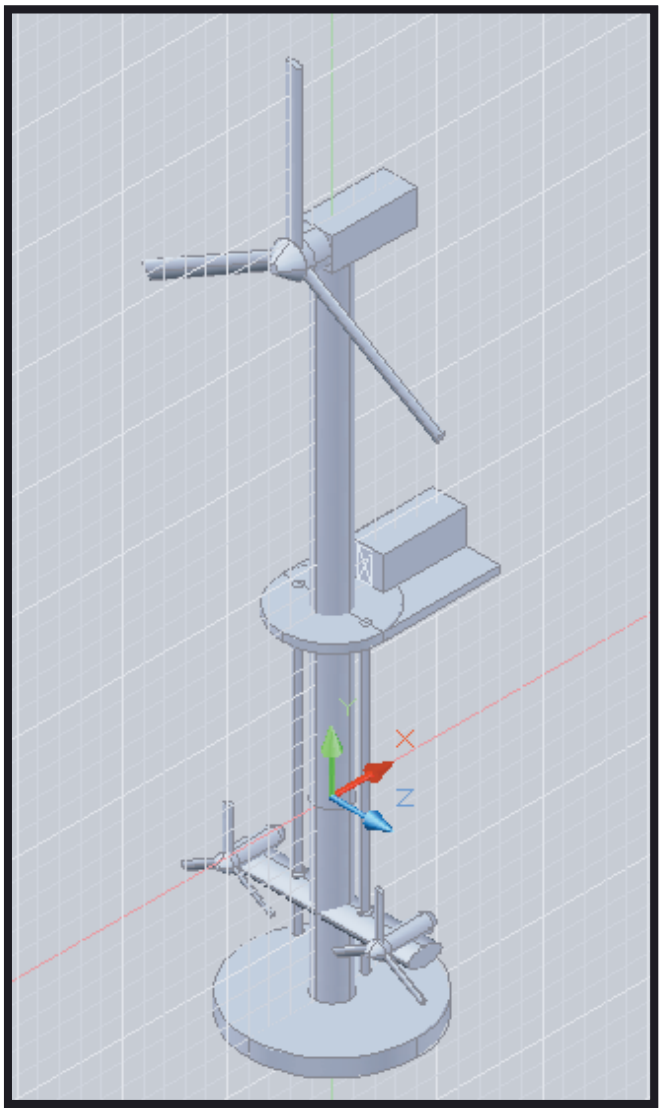

Figure 1: Isometric view of a dual offshore wind and tidal turbine.

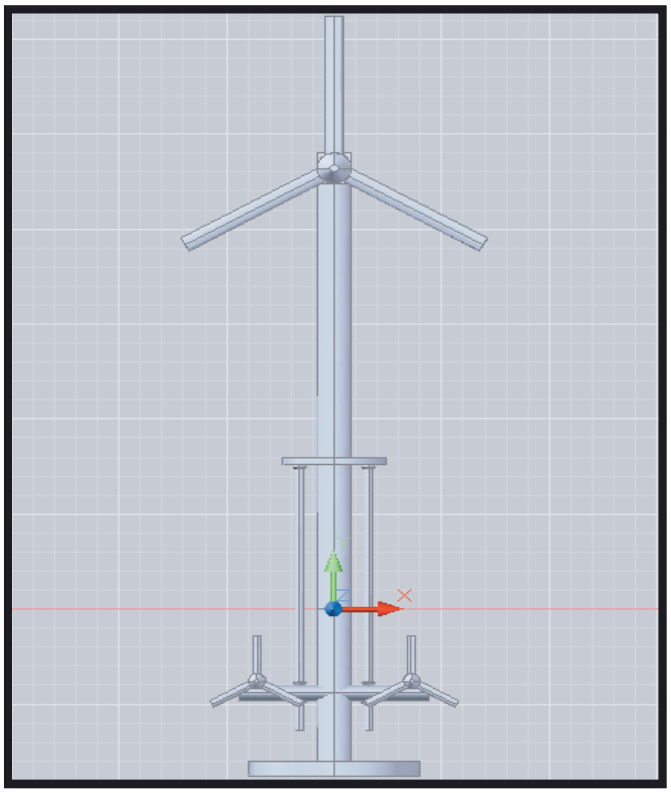

Figure 2: Front view of a dual offshore wind and tidal turbine.

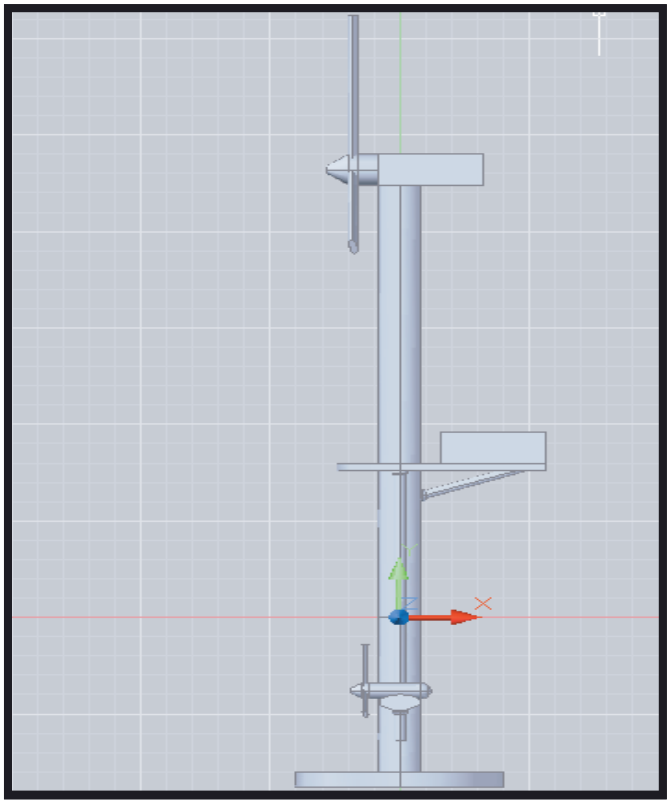

Figure 3: Side view of an offshore wind and tidal turbine.

6 Results and Discussion

	Wave Spectral Analysis					
	Case 1	Case 2	Case 3	Case 4	Case 5	Case 6
Hs	3.5	4	5	8	3.5	8
Tz	5	5	5	5	10	10

Table 1: Wave height and mean crossing period of 6 case studies.

Frequency		Case 1		Case 2		Case 3		Case 4		Case 5		Case 6	
f	σ_H	$S_{\eta\eta}$	$S_{\sigma\sigma}$	$S_{\eta\eta}$	$S_{\sigma\sigma}$	$S_{\eta\eta}$	$S_{\sigma\sigma}$	$S_{\eta\eta}$	$S_{\sigma\sigma}$	$S_{\eta\eta}$	$S_{\sigma\sigma}$	$S_{\eta\eta}$	$S_{\sigma\sigma}$
0.05	0	0	0	0	0	0	0	0	0	1.915	0	10.006	0
0.1	2	0.958	3.831	1.251	5.003	1.954	7.817	5.003	20.013	7.091	28.363	37.045	148.18
0.15	4	7.511	120.172	9.81	156.959	15.328	245.249	39.24	627.836	1.205	19.288	6.298	100.769
0.2	6	3.545	127.632	4.631	166.703	7.235	260.473	18.523	666.81	0.299	10.751	1.56	56.167
0.25	3	1.402	12.617	1.831	16.48	2.861	25.75	7.324	65.919	0.099	0.891	0.517	4.656
0.3	1	0.603	0.603	0.787	0.787	1.23	1.23	3.149	3.149	0.04	0.04	0.209	0.209
0.35	0	0.287	0	0.375	0	0.586	0	1.5	0	0.019	0	0.097	0
0.4	0	0.149	0	0.195	0	0.305	0	0.78	0	$9.5*10^{-3}$	0	0.05	0

Table 2: Wave Spectral Analysis.

	Case 1	Case 2	Case 3	Case 4	Case 5	Case 6
m_0	13.243	17.297	27.026	69.186	2.967	15.499
T_{zs}	5.521	5.521	5.521	5.521	7.011	7.011
Stress cycles to complete failure	$2.973*10^8$	$1.99*10^8$	$1.02*10^8$	$2.498*10^7$	$2.804*10^9$	$2.348*10^8$
Yearly Damage	0.019	0.029	0.056	0.23	$1.61*10^{-3}$	0.019
Fatigue Life	52.013	34.845	17.841	4.356	623.024	52.172

Table 3: Wave Spectral Analysis.

Table 1 above is based on the spectrum analysis carried out in this study; the table shows 6 different cases, each at a certain significant wave height (Hs) and a mean zero crossing periods (Tz). There measurement is taken at 8 frequencies with an increment of 0.05 Hz.

The first step as indicated in Table 2 is to calculate the wave amplitude spectrum($S_{\eta\eta}$); this is done by using the Pierson-Moskowitz spectrum

$$S_{\eta\eta}(f) = \frac{H_S^2}{4\pi T_Z^4 f^5} exp\left\{-\frac{1}{\pi}(fT_Z)^{-4}\right\} \quad \textbf{(19)}$$

The values of the stress (σ) have been given and together with $S_{\eta\eta}$ the stress response spectrum $S_{\sigma\sigma}$ can be written as follow:

$$\underbrace{S_{\sigma\sigma}(f)}_{\substack{Stress\ Response\\ Spectrum}} = \underbrace{|G(f)|^2}_{\substack{Transfer\\ Function}} \times \underbrace{S_{\eta\eta}(f)}_{\substack{Water\ surface\\ Elevation\\ Spectrum}} \quad \textbf{(20)}$$

In Table 3 the variance (m_0) is calculated which represents the area under the stress spectrum curve. At this point progress is made on to calculate the mean zero crossing period (T_{ZS}) of the stress response spectrum. After that the stress cycles to complete failure can be calculated, and later calculate the yearly damage, and the fatigue life. Depending on Hs and Tz the system will respond according to the wave characteristics, which will also influence the service life of the system.

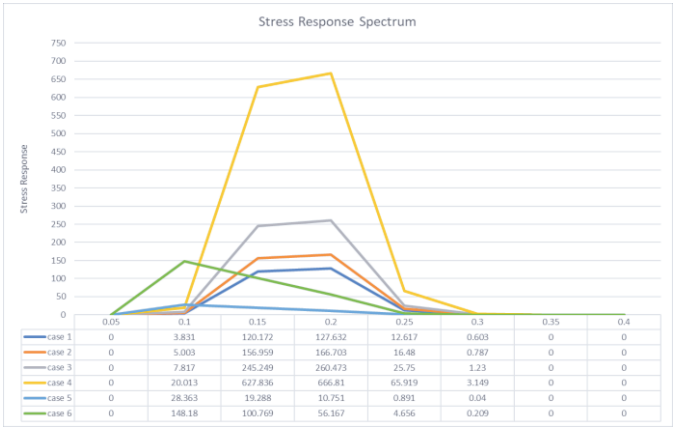

Figure 4: Stress Response Spectrum.

In Figure 4 above the stress response against frequency for 6 different cases which is known as a stress response spectrum. In the data below the chart the 6 different cases each corresponding to a certain significant wave height (Hs) and a mean zero crossing periods (Tz) are represented for the tidal turbine. The corresponding cells are there to show the stress response at each frequency.

The change in frequency is at an increment of 0.05 Hz, and is constant for all cases. For the first 4 cases a Tz of 5 seconds and varying Hs of 3.5, 4, 5, 8 m has been taken. From the chart with increasing wave height the stress on the structure will also increase and the response will be greater. For cases 5 and 6 Hs are given as 3.5, and 8, whereas the period is given 10 seconds. For case 5 the behavior is steady, because Tz of the wave is significantly higher than Hs this means the waves are less erratic. Incidentally this means that the structure barely feels the effect of the waves. For case 6 Hs is 8 m, this means the waves are more violent, and as can be seen the structure will respond to the wave effect but not so readily as for the first four cases because the Tz is twice as high, and therefore the waves are calmer.

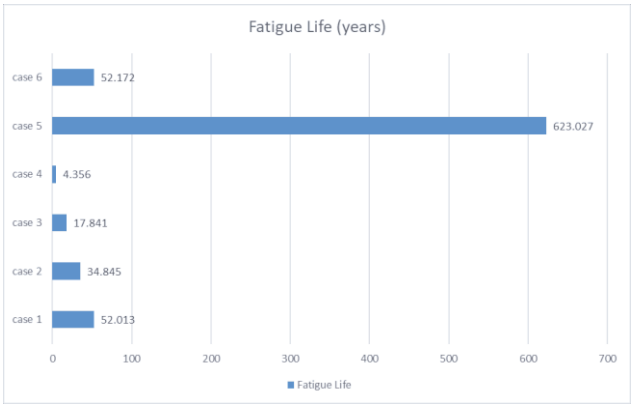

Figure 5: Fatigue life of the dual turbine.

Figure 5 above shows a bar chart of the fatigue life in years taking into account all 6 cases. For the first four cases at Tz of 5 seconds, the wave height is 3.5, 4, 5, and 8 m. clearly since the wave height increases so does its effect on the structure therefore reducing its fatigue life. Tz also has a role to play as it stands for the time the wave spends over the mean waterline. For cases 5 and 6 the Tz is 10 seconds, and Hs are 3.5, and 8. For case 5 since the wave spends twice as much time over the mean waterline compared with case 1 this means that it has a bigger wavelength, and that the propagation of the wave is not very rapid, therefore resulting in smaller response and a longer fatigue life. Case 6 is similar to case 4 except that Tz is doubled, this exhibits a similar behavior to case 5, the wave spends more time over the mean waterline, compared to case 4 and the propagation is less obvious, but since the wave height is larger than case 5 the waves will come in contact with a larger area along the structures vertical height and therefore the fatigue life is shortened.

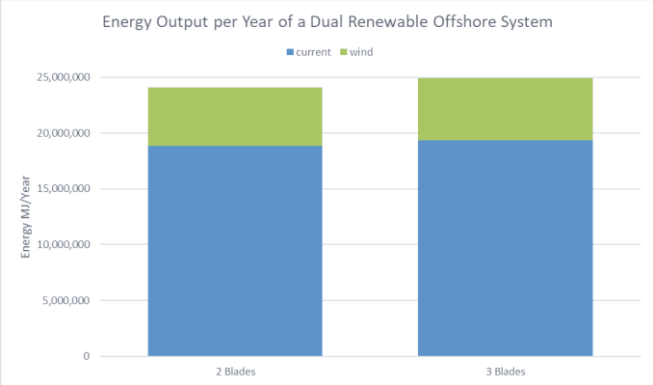

Figure 6: Energy per year of a dual offshore renewable energy system.

Figure 6 shows a stacked bar chart where the annual energy by a wind/tidal turbine used in this project for 2-blade and 3-blade and is based on the AutoCAD drawings from Figure 1-3. Based on the MathCAD simulation a 3 bladed turbine will produce slightly more power compared with the 2-blade one. This is because the windage area which comes in contact with the wind is greater for the 3-blade, due to the availability of an extra blade. The difference in generated power may not be large, but the extra amount of power generated by the 3-blade is significant nonetheless and corresponds to approximately 293,000 MJ a year. The concept and the MathCAD simulation of tidal turbine is similar to that of wind, the only difference is the fluid density. A tidal turbine will result in higher power per revolution because the fluid it is dealing with is denser, incidentally a tidal turbine will face difficulties with installation, and cavitation. Similar to the discussion of the wind energy, a 3 bladed turbine will produce slightly more power compared with the 2-blade one. This is because the area which comes in contact with the current is greater for the 3-blade, due to the availability of an extra blade. The difference in generated power may not be large, but the extra amount of power generated by the 3-blade is significant nonetheless and corresponds to approximately 550,000 MJ a year.

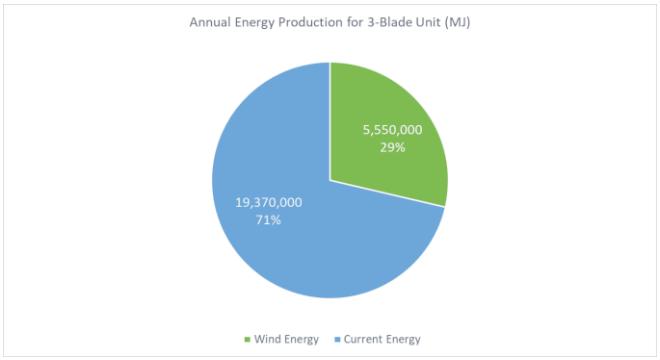

Figure 7: Energy distribution per 3 bladed wind/tidal turbine system.

Figure 7 pie chart considers the entire system composing of a 3-blade wind turbine, and a twin 3-blade tidal turbines which had been given in the design particulars and shown in the AutoCAD design figure 1-3. The amount of power produced from current energy is significantly higher and corresponds to about 71% of the total annual energy production. Whereas wind energy yield short of 30% of the total annual power production. The rotor diameter for the tidal turbine is 12 m which is much smaller than the 40 m diameter of the wind turbine, however since the density of the fluid is much greater (approximately 1000 times greater) the energy production with each revolution will also be greater, therefore a smaller rotor is needed. On the other hand, it is advisable to have a smaller rotor and shorter blades for a tidal turbine, due to the increase in pressure with depth might cause installation problems, also the loads on the rotor blades will vary with each revolution as the blades rotates between low-high pressure mediums.

7 Conclusion

This research concentrated its attention on the more widely used wind energy and on a lesser scope tidal energy. Many industries have started taking these two concepts to be their major energy supply resources from which they benefit.

The purpose of this study is to check the feasibility of connecting a wind turbine to a tidal turbine assuming that sufficient a simultaneous flow of wind and current mediums in any particular region whilst also taking into account the affiliated studies connected with the system. The considerations needed to be taken when one type is considered are similar to those when both units are put together, more specifically the flow velocity were assumed similar due to the wind effect on wave in a shallow location. this report attempted to cover the major difficulties this study would have to deal with, certain issues involving stress, power generation, fatigue and fracture, and wave spectrum analysis; all relevant topics related to installation, power grid, electrical connection, transportation, construction procedure, economics, have all been omitted from this report due to word constraint.

Due to the sheer size of the study and the immature experience in this field, this report merely reintroduced known facts about energy turbines. All influences made were at a smaller scale, there are concise books dedicated to each of the sections mentioned above, in fact in terms of hydrodynamics there are literatures which are dedicated to flow around circular cylinder only. In a project sense this report has elaborated on the necessary elements involved in a concept offshore wind/tidal turbine.

8 Acknowledgments

This research was supported by Khalifa University of Science and Technology and Research and by the department of Naval Architecture, Ocean and Marine Engineering at the University of Strathclyde Glasgow. Special thanks to our mentor Professor Nigel Barltrop from Strathclyde who provided insight and expertise that greatly assisted the research.

9 References

Achenback E. Distribution of local pressure and skin friction around a circular cylinder in cross-flow up to Re =5X106 [Journal] // Journal of Fluid Mechanics. - Germany : [s.n.], 1968. - Vol. 34.

Aggarwal Ankit [et al.] Irregular Wave Forces on a Large Vertical Circular Cylinder [Journal] // Energy Procedia. - Norway : ELSEVIER, 2016.

Ahlstrom Anders Aeroelastic Simulation of Wind Turbine Dynamics [Report] / Department of Mechanics ; Royal Institute of Technology. - Stockholm : Royal Institute of Technology, 2005.

Ainsile J. F. Calculating the Flow Field in the Wake of Wind Turbines [Journal] // Journal of Wind Engineering and Industrial Aerodynamics. - Amsterdam : Elsevier Science Publishers B.V., 1988. - Vol. 27.

An Hongwei, Cheng Liang and Zhao Ming Direct numerical simulation of oscillatory flow around a circular cylinder at low Keulegan–Carpenter number [Journal] // Journal of Fluid Mechanics. - Australia : Cambridge University Press 2010, 2010. - Vol. 666.

Barltrop Nigel and Adams Adrian Dynamics of Fixed Marine Structures [Book]. - Oxford : Elsevier Butterworth Heinemann, 1991. - Third Edition. - 978-07506-1046-9.

Beji S. Applications of Morison's equation to circular cylinders of varying cross-sections and truncated forms [Journal] // Ocean Engineering. - Turkey : ELSEVIER, 2019. - Vol. 187.

Bianchi Fernando D., Battista Hernan De and Mantz Ricrardo J. Wind Turbine Control Systems Principles, Modelling and Gain Scheduling Design [Book]. - London : Springer-Verlag London, 2007. - 1-84628-492-9.

Cao Shuyang, Li Ming and Cao Jinxing Numerical study of the flow over a circular cylinder in oscillatory flows with zero and non-zero mean velocity [Report]. - Korea : 2014 World Congress on Advances in Civil, Environmental, and Materials Research, 2014.

Chaviaropoulos P. K. and Hansen M. O. L. Investigating Three-Dimensional and Rotational Effects on Wind Turbine Blades by Means of a Quasi-3D Navier-Stokes Solver [Journal] // Journal of Fluid Engineering. - [s.l.] : ASME, 2000. - Vol. 122.

Christiansen J. P. Numerical Simulation of Hydrodynamics by the Method of Point Vortices [Journal] // JOURNAL OF COMPUTATIONAL PHYSICS . - England : [s.n.], 1971. - Vol. 135. - ARTICLE NO. CP975701.

Deng Xiaokang [et al.] Numerical simulations of free-surface waves past two vertically aligned horizontal circular cylinders [Journal] // Ocean Engineering. - [s.l.] : ELSEVIER, 2019. - Vol. 172.

Gamett Alan The Application of Statistical Concepts to the Wind Loading of Structures [Report] / Department of Civil Engineering ; University of Western Ontario. - Davenport : University of Western Ontario, 1960.

Gilbert B. L. and Foreman K. M. Experiments With a Diffuser Augmented Model Wind Turbine [Journal] // Energy Sources Technology Conference and Exhibition,. - New Orleans : ASME, 1983. - Vol. 105.

Giorgi Giuseppe and Ringwood John V. Analytical representation of nonlinear Froude-Krylov forces for 3-DoF point absorbing wave energy devices [Journal] // Ocean Engineering. - Ireland : ELSLEVIER, 2018. - Vol. 164.

Giorgi Giuseppe and Ringwood John V. Nonlinear Froude-Krylov and viscous drag representations for wave

energy converters in the computation/fidelity continuum [Journal] // Ocean Engineering. - Ireland : ELSEVIER, 2017. - Vol. 141.

Guven O., Farell C. and Patel V.C. Surface-roughness effects on the mean flow past circular cylinders [Journal] // Journal of Fluid Mechanics. - 1980.

Hansen M. O. L. [et al.] A global Navier-Stokes rotor prediction model [Report] / American Institute of Aeronautics and Astronautics, Inc.. - Reno : American Institute of Aeronautics and Astronautics, Inc., 1997. - A9715945.

Hansen M. O. L., Sørensen N. N. and Flay R. G. J. Effect of Placing a Diffuser around a Wind Turbine [Journal] // WIND ENERGY. - Denmark : John Wiley & Sons, Ltd., 2000. - Vol. 3.

Hansen M.O.L. [et al.] State of the art in wind turbine aerodynamics and aeroelasticity [Journal] // Progress in Aerospace Science. - Denmark : ELSEVIER, 2006. - Vol. 42.

Hansen Martin O. L. Aerodynamics of Wind Turbines [Book]. - London : Earthscan, 2008. - Second Edition. - 978-1-84407-438-9.

Hansen Morten H. [et al.] Control design for a pitch-regulated, variable speed wind turbine [Report] / Wind Energy Department ; Rise National Laboratory. - Denmark : DTU Library, 2005. - 87-550-3409-8.

Hau Erich Wind Turbines Fundamentals, Technologies, Application, Economics [Book]. - Berlin : Springer-Verlag Berlin, 2006. - Second Edition. - 3-540-24240-6.

Hayat Imran [et al.] Exploring wind farms with alternating two- and three-bladed wind turbines [Journal] // Renewable Energy. - USA : ELSEIVER, 2019. - Vol. 138.

Jordan Stanley K. and Fromm Jacob E. Oscillatory Drag, Lift, and Torque on a Circular Cylinder in a Uniform Flow [Journal] // The Physics of Fluids. - U.S.A. : AIP Publishing, 1972. - Vol. 15.

Kaffash M.H., Ganji D.D. and Nobakhti M.H. An analytical solution of turbulent boundary layer fluid flow over a flat plate at high Reynolds number [Journal] // Journal of Molecular Liquids. - Iran : ELSEVIER, 2017. - Vol. 230.

Kawaguti Mitutosi Numerical Solution of the Navier-Stokes Equations for the Flow Around a Circular Cylinder at Reynolds Number 40 [Journal] // Journal of Physical Society of Japan. - Japan : Physical Society of Japan, 1953. - Vol. 8.

Lee Cheol-Min [et al.] Effects of diffraction in regular head waves on added resistance and wake using CFD [Journal] // International Journal of Naval Architecture and Ocean Engineering. - South Korea : The Society of Naval Architecture of Korea, 2019. - Vol. 11.

Leonard A. Vortex Methods for Flow Simulation [Journal] // Journal of Computational Physics. - California : NASA, 1980. - Vol. 37.

Li Ai-jun and Liu Yong New analytical solutions to water wave diffraction by vertical truncated cylinders [Journal] // International Journal of Naval Architecture and Ocean Engineering. - China : Society of Naval Architects of Korea, 2019. - Vol. 11.

Lin Shangfei and Sheng Jinyu Assessing the performance of wave breaking parameterizations in shallow waters in spectral wave models [Journal] // Ocean Modelling. - Canada : ELSEVIER, 2017. - Vol. 120.

Lin Zi and Sayer P. An Enhanced Stiffness Model for Elastic Lines and its Application to the Analysis of a Moored Floating Offshore Wind Turbine [Journal] // Ocean Engineering. - Glasgow : ELSEVIER, 2015.

Lissaman P. B. S. Energy Effectiveness of Arbitrary Arrays of Wind Turbines [Journal] // Aerospace Sciences Meeting. - U.S.A. : American Institute of Aeronautics and Astronautics, 1979. - Vol. 3. - ARTICLE NO. 79-0114R.

Maull D.J. and Milliner M.G. Sinusoidal Flow Past a Circular Cylilnder [Journal] // coastal Engineerin. - Great Britain : ELSEVIER, 1978. - Vol. 2.

NASA MOD-2 Wind Turbine System Concept and Preliminary Design Report [Report] / National Aeronautics and Space Adminstration. - Cleveland : National Aeronautics and Space Adminstration, 1979. - NASA CR. 159609.

Newman John Nicholas Marine Hydrodynamics [Book]. - Cambridge : Massachusetts Instittute of Technology, 1977. - 978-0-262-14026-2.

O'Leary Kieran, Pakrashi Vikram and Kelliher Denis Optimization of composite material tower for offshore wind turbine structures [Journal] // Renewable Energy. - Ireland : ELSEIVER, 2019. - Vol. 140.

Perić Robinson and Abdel-Maksoud Moustafa Generation of free-surface waves by localized source terms in the continuity equation [Journal] // Ocean Engineering. - Germany : ELSEVIER, 2015. - Vol. 109.

Resio Donald T., Vincent Linwood and Ardag Dorukhan Characteristics of directional wave spectra and implications for detailed-balance wave modeling [Journal] // Ocean Modelling. - U.S.A. : ELSEVIER, 2015. - Vol. 103.

Rodrigues J.M. and Soares C. Guedes Froude-Krylov forces from exact pressure integrations on adaptive panel meshes in a time domain partially nonlinear model for ship motions [Journal] // Ocean Engineering. - Portugal : ELSEVIER, 2017. - Vol. 139.

Ruzzo Carlo, Saha Nilanjan and Arena Felice Wave spectral analysis for design of a spar floating wind turbine in Mediterranean Sea [Journal] // Ocean Engineering. - [s.l.] : ELSEVIER, 2019.

Sarpkaya Turgut A discrete-vortex analysis of flow about stationary and transversely oscillating circular cylinders [Report]. - California : Naval Postgraduate School, 1979. - NPS-69SL79011.

Sarpkaya Turgut Computational Methods With Vortices - The 1988 Freeman Scholer Lecture [Journal] // Journal of Fluid Engineering. - U.S.A. : ASME, 1989. - Vol. 111.

Stepanov Eugene and DarioTrevisan Three superposition principles: Currents, continuity equations and curves of measures [Journal] // Journal of Functional Analysis. - [s.l.] : ELSEVIER, 2016. - Vol. 272.

Sumer B. Mutlu and Fredsoe Jorgen Hydrodynamics Around Cylindrical Structures [Book]. - Singapore : World Scientific Publishing, 2006. - Revised Edition. - 981-270-039-0.

Sundar R. M. and Sullivan J. P. Performance of Wind Turbine in a Turbulent Atmosphere [Journal] // Solar Energy. - U.S.A. : Pergamon Press Ltd., 1982. - Vol. 31. - 0~38-092Xt83 53.00- 00.

Vasan Vishal and Deconinck Bernard The Bernoulli boundary condition for traveling water waves [Journal] // Applied Mathematics Letters. - U.S.A. : ELSEVIER, 2012. - Vol. 26.

Wang Piguang [et al.] Analytical solution for the short-crested wave diffraction by an elliptical cylinder [Journal] // European Journal of Mechanics / B Fluids. - China : ELSEVIER, 2019. - Vol. 74.

Wang Zizhe and Low Ying Min Analysis of the extreme wave elevation due to second-order diffraction around a vertical cylinder [Journal] // Applied Ocean Research. - Singapore : ELSEVIER, 2019. - Vol. 86.

Wilson Robert E. and Lissman Peter B.S. Applied Aerodynamics of Wind Power Machines [Report] / Oregon State University. - Oregon : Oregon State University, 1974. - Grant N.O G1-418340.

Wu Hao and Lin Yan An experimental investigation of the characteristics of a cylinder interacting with waves and flow in the dominant-load regime [Journal] // Applied Ocean Research. - China : ELSEVIER, 2019. - Vol. 89.

Zhang J. and Dalton C. A Numerical Comparison of Morison Equation Coefficients for Low Keulegan-Carpenter Number Flows; Both Sinusoidal and Nonsinusoidal [Journal] // Journal of Fluids and Structures. - U.S.A. : [s.n.], 1992.